Available online at www.sciencedirect.com
SCIENCE DIRECT
ELSEVIER
Journal of the European Ceramic Society 26 (2006) 2337–2344
ECERS
www.elsevier.com/locate/jeurceramsoc

Investigation of local orientation and stress analysis of PZT-based materials using micro-probe polarized Raman spectroscopy

Marco Deluca [a,b], Tatsuo Sakashita [c], Carmen Galassi [a], Giuseppe Pezzotti [b,*]

[a] *ISTEC-CNR, Institute of Science and Technology for Ceramics, via Granarolo, 64 I-48018 Faenza, Italy*
[b] *Research Institute for Nanoscience, Kyoto Institute of Technology, Matsugasaki, Sakyo-ku, 606-8585 Kyoto, Japan*
[c] *Taiyo Yuden Co. Ltd., 5607-2 Nakamuroda Haruna-machi, Gunma-gun, 370-3347 Gunma, Japan*

Received 21 January 2005; received in revised form 29 March 2005; accepted 14 April 2005
Available online 16 June 2005

Abstract

Investigation of crystallographic orientation and the related residual stress fields stored in piezoelectric sensor/actuator devices would improve reliability of industrial products and help to optimize the entire production process. Micro-probe Raman piezospectroscopy is a very attractive technique, yet not applied to lead zirconate titanate (PZT)-based materials, as the response is convoluted into contributions arising not only from stress, but also from crystallographic orientation. In this work, we have attempted to evaluate the correlation between Raman spectra and orientation in two differently doped lead zirconate titanate materials (PZT–LN and PZT–NSY), finding in the "softer" PZT a correlation between crystal orientation and Raman shift. We performed also some calibration experiments, and a piezospectroscopic (PS) coefficient has been retrieved in the "harder" PZT.

Keywords: Raman piezospectroscopy; Ferroelectric properties; PZT

1. Introduction

Lead zirconate titanate (PZT) is one of the most studied ferroelectric materials, due to its extremely wide field of applications as piezoelectric material. PZT possesses the highest coupling coefficient between electrical and mechanical properties, especially in the compositions between 0.4 and 0.6 mole fraction of $PbTiO_3$. The phase diagram of PZT shows that at these concentration values a morphotropic phase boundary (MPB) exists,[1] and is associated with a phase coexistence region, whose width depends on the compositional homogeneity and on the sample processing conditions[2]; this confers to the polycrystalline material the highest capability of orientation among ferroelectric ceramics.[3] Recently, Noheda et al.[2] discovered that a monoclinic phase is available in the MPB region of highly homogeneous samples cooled below ambient temperature. Doping of PZT can be performed by substitution of off-valent donors or acceptors, or isovalent additives; donors like Nb^{5+} replacing Zr^{4+} or La^{3+} replacing Pb^{2+} produce A-site vacancies in the perovskite, enhancing the mobility of domain walls. This may result in higher piezoelectric coefficients and permittivity, while mechanical properties are reduced; thus, donor-doped lead zirconate titanate is known as "soft" PZT. Acceptors such as Fe^{3+} replacing Zr^{4+} or Ti^{4+} are compensated by oxygen vacancies, which can move in the oxygen sublattice and form reorientable dipoles with the dopant cations: this stabilizes domain configuration and inhibits reorientation ("hard" PZTs). Isovalent additives (for example Ba^{2+} or Sr^{2+} replacing Pb^{2+}) usually produce inhibited domain reorientation and lower the Curie temperature.[3–5]

Applications of PZT range from power generation to pressure sensors in the security industry and actuators used as valves for electronic (ink jet printer heads), automotive (diesel common rail system), aeronautic and space industry (gas or fuel injection); PZT is well known also for ultra-

* Corresponding author. Fax: +81 75 724 7568.
E-mail address: pezzotti@chem.kit.ac.jp (G. Pezzotti).

0955-2219/$ – see front matter © 2005 Elsevier Ltd. All rights reserved.
doi:10.1016/j.jeurceramsoc.2005.04.016

Table 1
Processing parameters and characteristics of materials

PZT	T_{sinter} (°C)	$T_{postHIP}$ (°C)	$P_{postHIP}$ (bar)	$\rho_{theoretical}$ (g/cm^3)	ρ_{green} (%$\rho_{theoretical}$)	$\rho_{sintered}$ (%$\rho_{theoretical}$)	$\rho_{postHIPed}$ (%$\rho_{theoretical}$)	σ_{max} (MPa)
LN	1250	950	1000	7.9	65.6	94.1	97.4	86.1 ± 11.2
NSY	1200	–	–	7.8	67.1	94.9	–	69.8 ± 2.2

sonic motors, liquid atomizers, acoustic applications, and transducers.[6] However, piezoelectric devices are affected by reliability problems, due mostly to the residual stress fields stored in the material during processing and operation. In particular, in multilayer actuators internal stress concentration during electric field application sometimes initiates cracks in the proximity of internal electrode edges[7]; more complicated and expensive design may improve the actuator reliability. Problems can arise also from local inhomogeneities of the mechanical stress field, not only in multilayer structures, but also in thin films or more complex textures; crack growth can be promoted during operation. For these reasons, residual stress measurements would provide important information about possible improvements in both the process and the device configuration; in addition, a technique capable to monitor product lifetime with a non-destructive control is highly desired. Residual stress measurement is usually performed by X-ray diffraction methods, although a trend toward even smaller-scale piezoelectric devices forces the development of new analytical methods to reveal micro- or even nano-scale residual stresses. Raman micro-probe piezospectroscopy is a well-known method for the analysis of residual stresses, applicable to a broad range of materials, especially ceramics. However, Raman piezospectroscopy has not yet been widely applied on PZT-based materials. In their pioneering work, Xu et al.[8] were able to examine PZT thin films by Raman spectroscopy, by invoking a theoretical background based on thermodynamic considerations. However, the fitting procedure they used to determine the phonon frequencies of their spectra (a searching rectangle tool) appears to be insufficient for the precise assessment of maximum band position needed in piezospectroscopic stress assessments. Li et al.[9] used polarized Raman spectroscopy to understand domain orientation in perovskitic $BaTiO_3$ and in $PbTiO_3$. Additional studies of Raman spectra in PZT materials differing in composition and manufacturing conditions have been performed[10–12]; these studies represent the backbone on which the fitting approximations adopted in this study were based.

The aim of this work was first to correlate the Raman spectra collected in soft and hard PZT-based materials (PZT–LN and PZT–NSY, respectively) with their local crystallographic orientation, and then to retrieve a PS coefficient. It is anticipated that we have been able to find a parameter for the characterization of local orientation (or the degree of orientation), and in the case of the softer PZT a correlation to determine crystallographic shift of selected Raman bands. Retrieval of PS coefficient has been also possible in the harder PZT.

2. Experimental and computational procedures

2.1. Materials

PZT–LN, lanthanum and niobium doped (composition $PbZr_{0.60}Ti_{0.40}O_3$ plus La 3.61 mol% and Nb 0.32 mol%), and PZT–NSY, niobium, strontium and yttrium doped (composition $PbZr_{0.54}Ti_{0.46}O_3$ plus Nb 0.60 mol%, Sr 4.47 mol% and Y 0.26 mol%) powders were prepared by solid state reaction of the starting oxides. The powder synthesis process was the following: (i) 48 h ball milling in water of the stoichiometric oxide amounts in a plastic jar with ZrO_2 milling media; (ii) freeze drying of the suspension; (iii) sieving at 250 μm; (iv) heat treatment in air at 850 °C for 4 h in a zirconia crucible; (v) wet ball milling in ethanol for 100 h using a plastic jar with ZrO_2 milling media; (vi) drying in oven at 90 °C; (vii) sieving at 250 μm. Powders were uniaxially dry pressed and then subjected to cold isostatic pressing at 3000 bar; sintering occurred at different conditions for the two materials in an alumina crucible, and $PbZrO_3$ was added to further prevent PbO volatilization; only PZT–LN was then subjected to post-hipping to enhance sintered density. Processing parameters and characteristics of green and sintered materials are summarized in Table 1. Density measurements were performed with the Archimede's method.

The sintered tablets were then cut in the shape of 25 mm × 3.2 mm × 3.0 mm bars; after polishing an Ag electrode was screen printed on 25 mm × 3.0 mm sides, and polymeric residuals were removed by heating at 750 °C. Poling process was performed for each sample in an oil bath at 120 °C, and a voltage sufficient to overcome the coercive field in the material (3 kV/mm) was applied for 85 min; before removal of electric field, samples were left for 45 min in the oil bath without temperature control (cooling proceeded until 60 °C). Measures of dielectric permittivity (ε_{33}) and piezoelectric coefficient (d_{33}) were performed with an impedance/gain phase analyzer (HP4194A, Hewlett-Packard) and a d_{33} Berlincourt meter (S5865 Sinocera, State College, PA, USA) and the results are listed in Table 2. Dopants as La^{3+} replacing Pb^{2+} and Nb^{5+} for Ti^{4+}–Zr^{4+} enhance domain walls mobility, while Sr^{2+} replacing Pb^{2+}

Table 2
Electrical properties of materials

	ε_{33}	d_{33} (10^{-12} CN^{-1})
PZT–LN	4023	696
PZT–NSY	2599	577

and Y^{3+} replacing Ti^{4+}–Zr^{4+} produce inhibited domain wall movement; in PZT–NSY the Nb^{5+} doping ensures a high d_{33}, but due to the substantial Sr^{2+} content and the presence of yttrium this material can be considered slightly "harder" than PZT–LN, and this is reflected by its lower d_{33} (Table 2).

2.2. Raman spectroscopy and piezospectroscopy

Raman measurements were performed with a T64000 spectrometer (Horiba/Jobin-Yvon - Kyoto, Japan), equipped with an Ar^+ laser (Stabilite 2017, Spectra Physics, Mountain View, CA, USA) operating at a wavelength of 488 nm. A liquid nitrogen cooled charge coupled device (CCD) detector was employed to acquire spectra, and the laser spot was focused on sample surface with 50× or 100× long-focus objectives, which allow a 13 and 6 mm working distance, respectively, and a lateral resolution of 2 and 1 μm, respectively. Polarization of the incident laser beam was selected parallel to the preferential domain orientation of samples (y), and spectra were collected in a strict backscattering geometry in parallel $z(yy)z$ and cross $z(yx)z$ configuration (according to Porto notation[13]) with a dichroic sheet polarizer; a half-wave plate was used to rotate $z(yy)z$ spectra in order to compensate for the polarization dependence of the monochromator. To measure spectra characteristics with respect to orientation of domains (angular calibration) a special procedure was chosen: a rotating stage was used, and the specimen was placed with its preferential domain orientation aligned (0°) or perpendicular (90°) with respect to incident laser beam polarization direction. Spectra were collected exactly on the same point with $z(yy)z$ and $z(yx)z$ configurations, every 10° of rotation from 0° to 180°; relative intensity of Raman modes $E(TO_2)$ and $E(LO_2)$ and wavenumber were plotted against the angular degree of rotation.

For the mapping of local orientation in the neighbourhood of an indentation a Vickers hardness tester (AVK-C1, Akashi Co., Zama, Japan) has been used with an applied load of 2.94 N.

PS calibration experiments were performed with the four-point bending technique on a special jig equipped with a micrometric screw; the applied load was monitored with a 100 kg_f load cell and the maximum applied stress was calculated according to the elastic beam theory. Spectra were collected along a line selected at the center of the bending bar and spanning from the tensile to the compressive side of the sample; the wavenumber shift versus applied stress was then plotted according to the recorded location.

The PS coefficient of a material can vary depending on both chemistry and thermal history of the specimen; different production procedures can lead to different response to applied stress. We decided to prepare model samples with different chemical composition, as the present technique has been applied for the first time. However, the spectroscopic methods shown in this study can be considered to own general validity and are also applicable to commercial materials.

Spectral shift of PZT Raman bands, as detected during application of stress in a piezospectroscopic calibration, can be considered to be the convolution of different contributions:

$$\Delta\upsilon = \Delta\upsilon_{res} + \Delta\upsilon_{cry_{res}} + \Delta\upsilon_{stress} + \Delta\upsilon_{cry_{stress}} + \Delta\upsilon_{relax} \quad (1)$$

where $\Delta\upsilon_{res}$ is the shift due to eventual residual stress fields in the sample prior to application of calibration load, $\Delta\upsilon_{cry_{res}}$ is the shift due to the crystallographic orientation referred to this condition, $\Delta\upsilon_{cry_{stress}}$ is the shift due to the crystallographic orientation induced by the applied stress (owing to ferroelastic effect), $\Delta\upsilon_{stress}$ is the shift due to applied stress, $\Delta\upsilon_{relax}$ refers to the stress relaxed as domain switching proceeds during application of load. If we acquire the "stress-free" wavenumber value on the same material (or even in a sample with the same manufacturing and stress history) before applying external stress, the first two shift contributions on the right hand of Eq. (1) are included in that value and can be neglected if the probe size allows statistical reproducibility in sampling the material microstructure (i.e., a sufficiently high number of grains are probed at each measurement). During the application of stress, the remaining contributions in Eq. (1) sum up, and the acquired wavenumber includes: (i) the shift due to the angle between laser polarization direction and the local average crystallographic orientation; (ii) the shift due to relaxing of stress during domain switching; and (iii) the shift caused by domain reorientation due to the externally applied stress itself. For these reasons, when the shift detected is simply diagrammed against the applied stress a highly scattered response is usually found, which can prevent from obtaining a linear relationship, and thus a single value of PS coefficient (i.e., the slope of the diagram of Raman shift versus stress). This calls for building up a suitable deconvolution procedure of the observed $\Delta\upsilon$ into a stress related component and a crystallographic orientation related component. A suitable procedure is for the first time proposed in this paper.

2.3. Fitting procedures

Raman spectra of PZT–LN and PZT–NSY are shown in Fig. 1a and b, respectively. Fitting procedures involved the use of two different commercially available software packages. The intensity values of phonon modes for both materials were obtained using Labspec 4.02 (Horiba/Jobin-Yvon) package, according to Gaussian–Lorentzian mixed functions after subtracting a baseline and applying the initial approximations of modes position according to the PZT Raman analysis given by Meng et al.[10]; an example of fitting is reported in Fig. 2. In PZT, it is extremely difficult to precisely obtain band maxima wavenumber values by using built-in picking peaks procedures commonly available in commercial software packages;

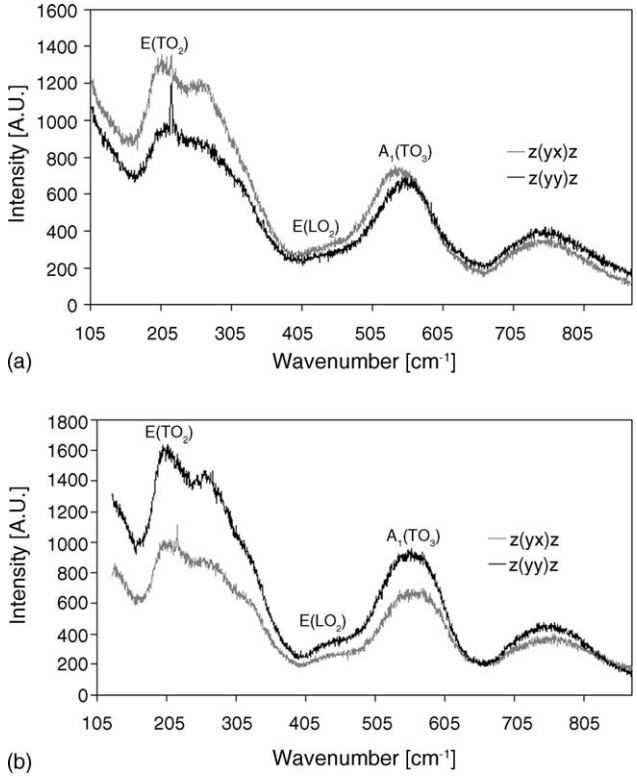

Fig. 1. Raman spectra of (a) PZT–LN and (b) PZT–NSY collected with parallel $z(yy)z$ and cross $z(yx)z$ configuration.

this is mainly because the Raman modes of PZT appear rather broad. For this reason we developed a fitting procedure capable to unambiguously retrieve wavenumber values of spectra maxima. We represented spectra in Origin 6.0 (Microcal Software Inc., Northampton, MA, USA) – (Fig. 3, for PZT–LN) – and performed a smoothing with FFT Filter tool, thus allowing to reduce noise significantly (Fig. 3a). After noise reduction, it was possible to obtain a clear derivative of the smoothed function, and to retrieve unambiguously the desired wavenumber just searching for the derivative zero point (Fig. 3b).

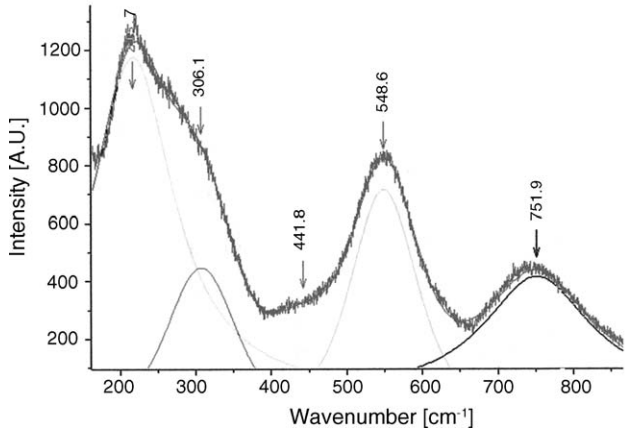

Fig. 2. Treatment of PZT–LN $z(yy)z$ spectrum with Labspec 4.02.

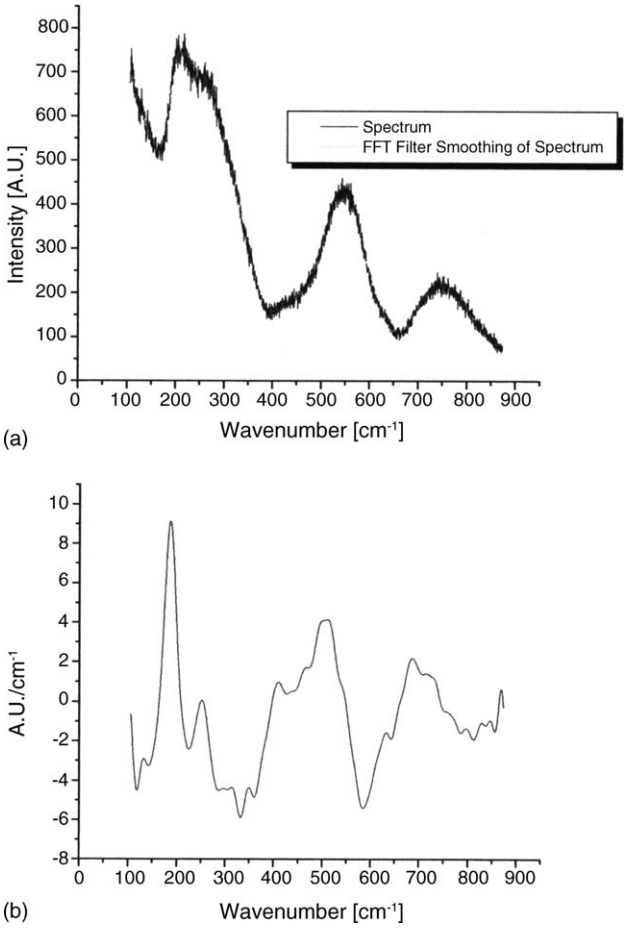

Fig. 3. Treatment of PZT–LN $z(yy)z$ spectrum with Origin 6.0: (a) FFT Filter smoothing of spectrum and (b) differentiation of the smoothed function.

3. Results and discussion

3.1. Calibration of domain orientation

Results for angular calibration of PZT–LN are shown in Fig. 4, where the $z(yy)z$ relative intensity of modes $E(TO_2)$ and $E(LO_2)$ versus degree of rotation of the stage used is plotted. As can be noted, the behaviour of 0° oriented samples (with respect to laser polarization direction) is complementary to the behaviour of 90° oriented samples. In fact, the laser probe focussed onto the sample surface with a 100× magnification excites the same volume at any rotation angle of the sample stage; the average of all the domain orientations invested by the laser beam is the local main preferential direction of the polarized sample. Zero degree sample (Fig. 4a) has its preferential orientation aligned with laser polarization only at 0°, 180°, 360°; 90° sample (Fig. 4b) has its preferential orientation aligned with laser polarization only at 90° and 270°. Therefore, it is demonstrated by the trends obtained in Fig. 4 that the relative intensity of Raman modes $E(TO_2)$ and $E(LO_2)$ is a parameter capable to detect the local orientation of ferroelectric domains in PZT-based materials. Regarding an unpoled sample, it can be easily noted that no preferential

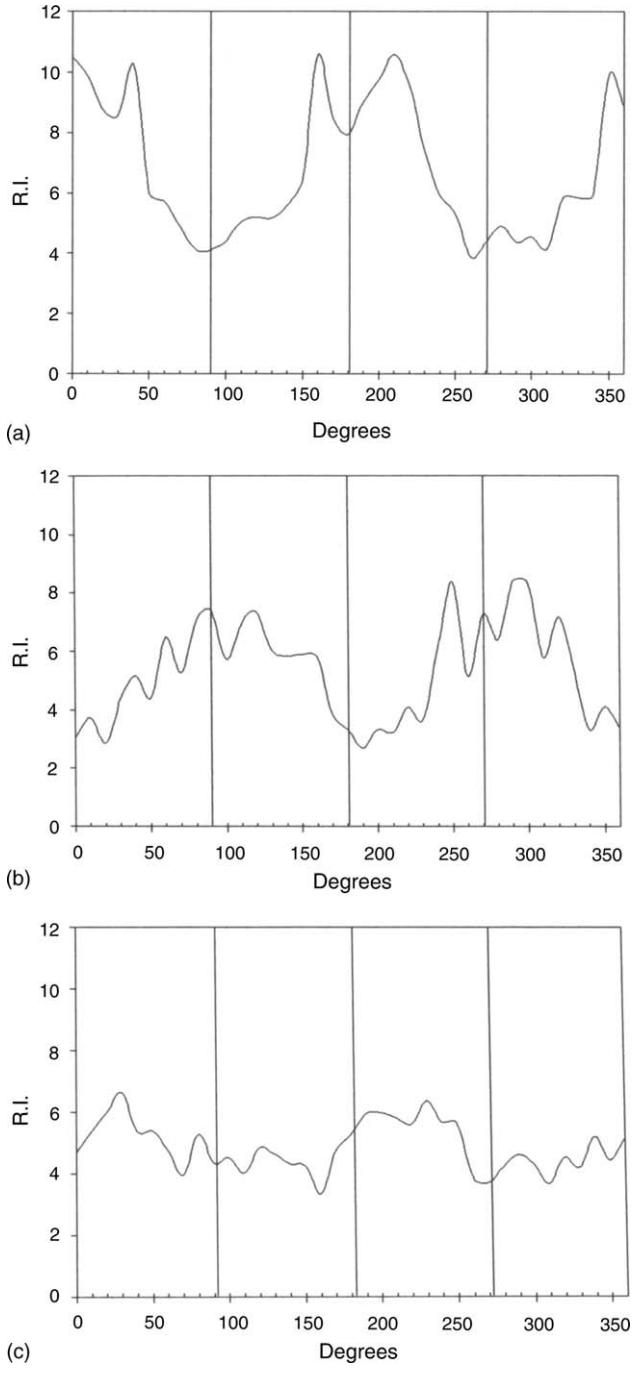

Fig. 4. Relative intensity of $E(TO_2)$ and $E(LO_2)$ modes vs. angle between local crystallographic orientation and the polarization direction of incident laser light for PZT–LN samples having their ferroelectric domains averagely aligned with incident light (a) at 0°, 180°, 360° (b) at 90°, 270° (c) unknown (unpoled sample).

orientation for the probed area is detectable and the results of the orientation calibration is highly scattered (Fig. 4c). These results are very similar to that obtained in single crystal perovskite crystals and indicate that the present polycrystalline PZT–LN, if poled, possesses a high degree of preferential orientation.

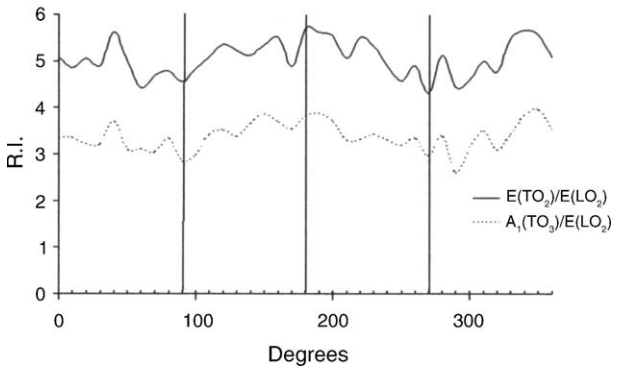

Fig. 5. Relative intensity of modes $E(TO_2)$ and $E(LO_2)$, $A_1(TO_3)$ and $E(LO_2)$ vs. angle between local average crystallographic orientation and the polarization direction of incident laser light for PZT–NSY (0° sample).

In PZT–NSY, the degree of orientation of 0° samples is less than that found in PZT–LN (Fig. 5), as the relative intensity of $E(TO_2)$ and $E(LO_2)$ modes appears more scattered and close to the unpoled sample behavior; this result is in agreement to the PZT–NSY characteristic of being slightly harder than PZT–LN, due to different doping. However, it is clear to notice that a preferential orientation is present in this material, as indicated also by the ratio of the intensity values of the $A_1(TO_3)$ and the $E(LO_2)$ modes; although the results are scattered, it can be easily noted that both curves in Fig. 5 have the same profile, comparable to the trend represented in Fig. 4a for 0° PZT–LN.

The plot of relative intensity (RI), versus the orientation angle (α), as that obtained for PZT–LN, has been fitted with the following sinusoidal function (Eq. (2)) with the aid of Origin 6.0 software (Fig. 6):

$$\mathrm{RI} = P + A \sin\left(\pi \frac{\alpha - x_c}{w}\right) \quad (2)$$

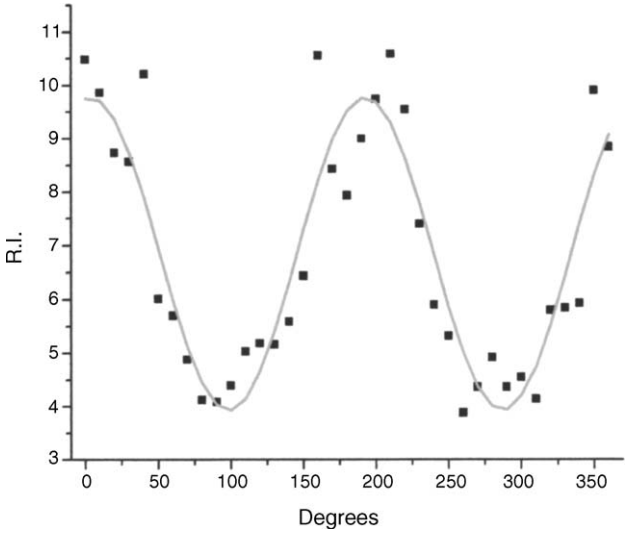

Fig. 6. Modelling of angular dependence of relative intensity in PZT–LN.

Table 3
Fitting parameters for Eq. (2)

	0° PZT–LN (RI vs. degree)	90° PZT–LN (RI vs. degree)	0° PZT–LN (wavenumber vs. degree)
P	6.85	5.23	215.27
A	2.92	−0.89	−2.45
x_c	145.37	250.74	167.70
w	94.33	2.57	45.71

where P is the position of the symmetry axis of the curve, parallel to x-axis, A is the amplitude of the wave, x_c is the abscissa center of the fitting curve, and w is the half-wave width. Table 3 summarizes the fitting parameters for 0° and 90° PZT–LN.

According to this correlation, it is possible to perform a mapping of angle of preferential orientation in selected areas of the PZT material, for example, around cracks and indentation prints. However, in order to do so, it is imperative to acquire spectra with the same objective lens according to which the angular correlation has been established, because a different magnification leads to different probe penetration depth and, therefore, to different volumetric averages of the orientation. We applied this correlation to a map collected near a Vickers indentation print (Fig. 7) on a PZT–LN material with the preferential orientation of domains perpendicular to the polarization direction of incident laser light (90° sample). The map enables one to visualize the effect of the indentation in terms of domain switching. As could be noted, far away from the indentation (represented as a homogeneous grey zone) the domains are unaffected and their orientation is nearly constant at 90°; gradually, by moving closer to the indentation print, the average orientation changed and areas in which the domains are fully switched by 90° can be visualized; in particular, nearby the tip of cracks generated from the corners of the indentation, the domains were fully switched; this is consistent with the presence of a tensile stress field generated during crack propagation around crack tips, according to which ferroelastic domain switching occurs parallel to the direction of tensile stress[14]; 90° switching occasionally occurred also away from the indentation crack, and this is supposed to be the effect of the presence of secondary cracks.

Wavenumbers of the E(TO_2) mode of PZT–LN and PZT–NSY 0° samples, both collected in the $z(yx)z$ configuration, are plotted versus angular degree in Fig. 8a and b, respectively. In the absence of an applied stress, the wavenumber shift recorded in poled PZT is simply the sum of two contributions: (i) the shift due to residual stress previously stored in the material (for instance, produced during the poling process) and (ii) the shift arising from the angular orientation between the average crystallographic axis and the polarization direction of the incident laser light. As the former does not vary with orientation, only the trend of the latter is represented in Fig. 8. A relationship is found in both materials, but only in PZT–LN it was possible to perform a fitting with a symmetrical equation. A symmetrical fitting (e.g., by a sinusoidal curve) is needed to obtain a value of crystallographic shift from measuring the relative intensity of the E(TO_2) and the E(LO_2) modes; in fact, from the correlation reported in Fig. 6, two possible values of orientations are retrievable. If a symmetrical correlation is found between degree of orientation and wavenumber shift, it is possible to assign to any couple of retrieved angles an unique value of crystal-

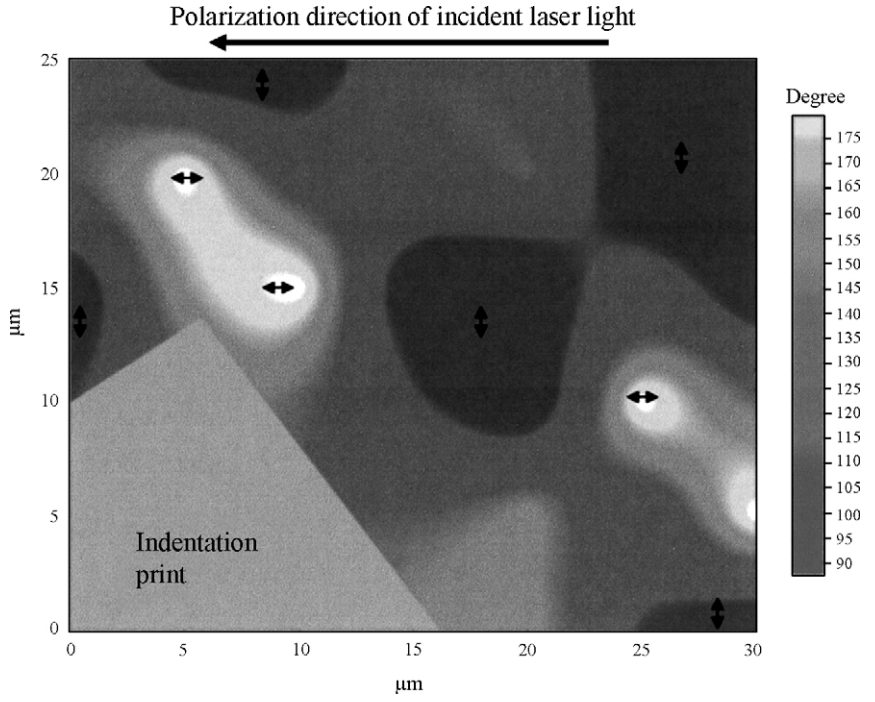

Fig. 7. Angular mapping of local orientation near a Vickers indentation in 90° oriented PZT–LN.

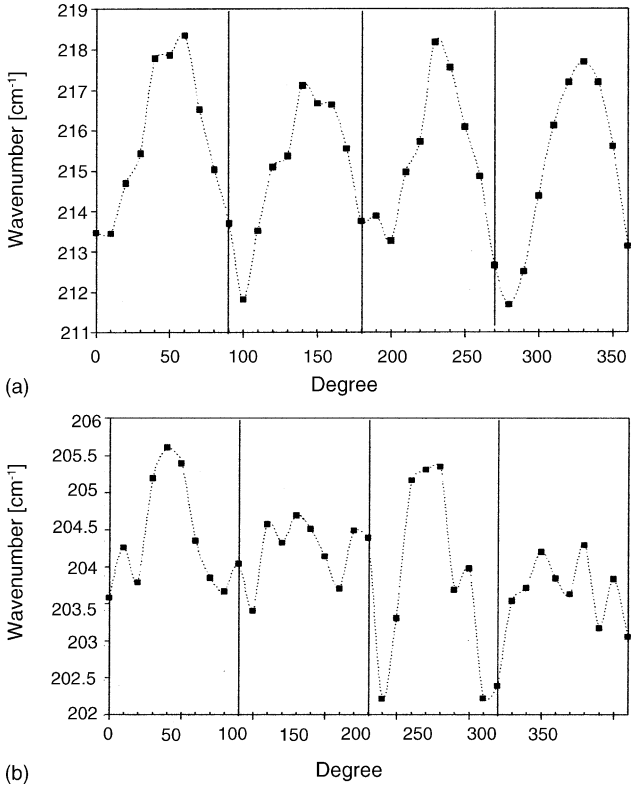

Fig. 8. Dependence of the wavenumber with respect to the angle between local average crystallographic orientation and the polarization direction of the incident laser light for (a) PZT–LN and (b) PZT–NSY.

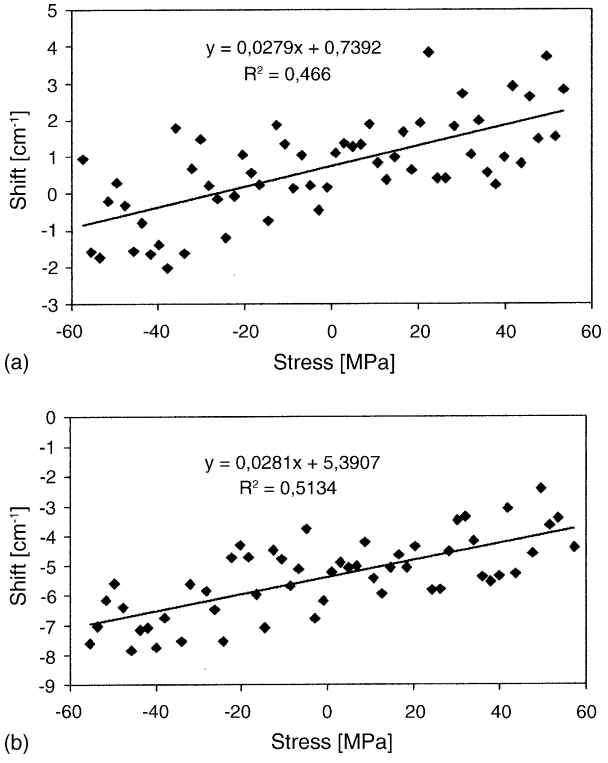

Fig. 9. Four-point bending calibrations for PZT–LN (a) before and (b) after deconvolution of wavenumber from crystallographic shift contribution.

lographic shift, and deconvolute the achieved wavenumber into a crystallographic related component and a stress related component. To fit the PZT–LN trend of wavenumber versus angular degree, an equation has been applied, which has the same form of Eq. (2) (see Table 3 for the fitting parameters used). Regarding PZT–NSY, a similar relationship could not be obtained.

3.2. Four-point bending calibration

Results of four-point bending calibration for PZT–LN are depicted in Fig. 9a. As seen from the plot, a linear relationship for this material was hardly retrievable, because the response of Raman shift was highly scattered; however, the application of the previously mentioned shift deconvolution (Fig. 9b) helps to isolate the contribution to shift given by the externally applied stress and, thus, allows to slightly improve the correlation. The error involved with considering the slope retrieved in PZT–LN as PS coefficient with respect to an unknown stress field is about 13.5% (as calculated with Origin 6.0 software). This behaviour can be attributed to the phenomenon of ferroelasticity: in ferroeleastic materials a domain switching occurs when subjected to external stress; an applied compressive stress favours dipole orientations perpendicular to the applied stress, while tension favours dipole orientation parallel to the applied stress.[5,14] In a polycrystalline material, the orientation of the crystallographic axes of the crystallites is initially random, and the domain reorientation inside each grain occurs within the boundary conditions imposed by the surrounding grains. For this reason, in a poled material the application of stress can result in increased disorder: the initial preferential orientation of domains is disturbed, as not all the domains invested by the superimposed external stress field receive the energy necessary for a complete switching. This behaviour is enhanced in materials in which the ferroelastic effect is dominant, like in the softer PZT-based materials, where the energy necessary for domain wall motion is extremely low. On the other hand, in the harder PZT–NSY material, the piezo-spectroscopic behavior was more reliable (Fig. 10). As could be noted, the correlation obtained is less scattered ($R^2 = 0.81$ against $R^2 = 0.51$). In PZT–NSY, the domain switching requires higher energy than PZT–LN, due to different doping. For this reason, locally the change in domain orientation is less extensive and the Raman shift is less affected; in PZT–NSY is therefore possible to retrieve a PS coefficient. The value of PS coefficient ($\Pi_u = -25.2\,\mathrm{cm}^{-1}/\mathrm{GPa}$) can be applied to residual stress analyses, and the error involved in considering this value with respect to unknown stress fields is less than 4%.

In conclusion, in a soft material, where ferroelasticity plays a major role, the results of piezospectroscopic calibration are somewhat scattered even though deconvolution between the stress and the crystallographic contributions is applied. In a harder material the rotation of crystallographic axes does not occur extensively, and we can obtain a less

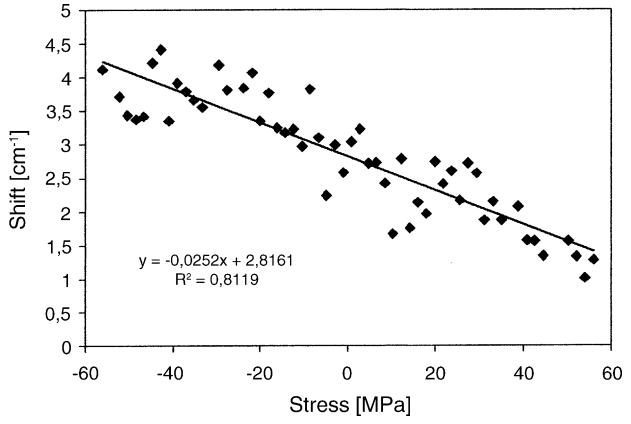

Fig. 10. Four-point bending calibration of PZT–NSY.

scattered piezo-spectroscopic response even though we lack a method to deconvolute crystallographic shift.

4. Conclusion

Two different PZT-based materials have been investigated by Raman spectroscopic and piezospectroscopic measurements. A correlation between relative intensity of Raman modes $E(TO_2)$ and $E(LO_2)$ and the angle between the local orientation of domains and the polarization direction of incident laser light has been retrieved. We demonstrated that local orientation of domains in PZT influences the Raman spectrum of the material, and a relationship between wavenumber shift and angular orientation of the crystallographic domains has been established; it is possible to obtain a value of crystallographic shift by measuring relative spectral intensity and applying the correlations found in this study. We also performed piezospectroscopic calibrations in a four-point bending configuration, and found that a linear relationship between wavenumber shift and applied stress is retrievable only in materials where domain wall movement is partly inhibited, and the ferroelastic effect is not predominant during calibration loading. A PS coefficient $\Pi_u = -25.2\,cm^{-1}/GPa$ has been found for PZT–NSY.

References

1. Jaffe, B., Cook jr., W. R. and Jaffe, H., *Piezoelectric Ceramics*. Academic Press, New York, 1971.
2. Noheda, B., Cox, D. E., Shirane, G., Gonzalo, J. A., Cross, L. E. and Park, S. E., A monoclinic ferroelectric phase in the $Pb(Zr_{1-x}Ti_x)O_3$ solid solution. *Appl. Phys. Lett.*, 1999, **74**(14), 2059–2061.
3. Setter, N., ABC of piezoelectricity and piezoelectric materials. In *Piezoelectric Materials in Devices*, ed. N. Setter. EPFL, Lausanne, 2002.
4. Haertling, G. H., Ferroelectric ceramics: history and technology. *J. Am. Ceram. Soc.*, 1999, **82**(4), 797–818.
5. Moulson, A. J. and Herbert, J. M., *Electroceramics: Materials Properties and Applications*. Chapman Hall, London, 1990.
6. Wersing, W., Application of piezoelectric materials: an introductory review. In *Piezoelectric Materials in Devices*, ed. N. Setter. EPFL, Lausanne, 2002.
7. Uchino, K., Designing piezoelectric actuators. In *Piezoelectric Materials in Devices*, ed. N. Setter. EPFL, Lausanne, 2002.
8. Xu, W. H., Lu, D. and Zhang, T. Y., Determination of residual stresses in $Pb(Zr_{0.53}Ti_{0.47})O_3$ thin films with Raman spectroscopy. *Appl. Phys. Lett.*, 2001, **79**(5), 4112–4114.
9. Li, Z., Foster, C. M., Dai, X. H., Xu, X. Z., Chan, S. K. and Lam, D. J., Piezoelectrically-induced switching of 90° domains in tetragonal $BaTiO_3$ and $PbTiO_3$ investigated by micro-raman spectroscopy. *J. Appl. Phys.*, 1992, **71**(9), 4481–4486.
10. Meng, J. F., Katiyar, R. S., Zou, G. T. and Wang, X. H., Raman phonon modes and ferroelectric phase transitions in nanocrystalline lead zirconate titanate. *Phys. Stat. Sol. A*, 1997, **164**, 851–862.
11. Haines, J., Roquette, J., Bornand, V., Pintard, M., Papet, Ph. and Gorelli, F. A., Raman scattering studies at high pressure and low temperature: technique and application to the piezoelectric material $Pb(Zr_{0.52}Ti_{0.48})O_3$. *J. Raman Spectr.*, 2003, **34**, 519–523.
12. Burns, G. and Scott, B. A., Raman spectra of polycrystalline solids; application to the $PbTi_{1-x}Zr_xO_3$ system. *Phys. Rev. Lett.*, 1970, **25**(17), 1191–1194.
13. Damen, T. C., Porto, S. P. S. and Tell, B., Raman effect in zinc oxide. *Phys. Rev.*, 1966, **142**(2), 570–574.
14. Fett, T., Munz, D. and Thun, G., Bending strength of a PZT ceramic under electric fields. *J. Eur. Ceram. Soc.*, 2003, **23**, 195–202.